



The Journal of Infectious Diseases

MAJOR ARTICLE

RNA landscapes of brain and brain-derived extracellular vesicles in simian immunodeficiency virus (SIV) infection and central nervous system pathology

Yiyao Huang^{1,2}, Ahmed Abdelgawad³, Andrey Turchinovich^{4,5}, Suzanne Queen¹, Celina Monteiro Abreu¹, Xianming Zhu⁶, Mona Batish³, Lei Zheng², Kenneth W. Witwer^{1,7,8*}

¹Department of Molecular and Comparative Pathobiology, Johns Hopkins University School of Medicine, Baltimore, MD, USA; ²Department of Laboratory Medicine, Nanfang Hospital, Southern Medical University, Guangzhou, Guangdong, China; ³Department of Medical and Molecular Sciences, University of Delaware, Newark, DE, USA; ⁴Division of Cancer Genome Research, German Cancer Research Center DKFZ, Heidelberg, Germany; ⁵Heidelberg Biolabs GmbH, Heidelberg, Germany; ⁶Department of Pathology, Johns Hopkins University School of Medicine, Baltimore, MD, USA; ⁷Department of Neurology, Johns Hopkins University School of Medicine, Baltimore, MD, USA; ⁸Richman Family Precision Medicine Center of Excellence in Alzheimer's Disease, Johns Hopkins University School of Medicine, Baltimore, MD, USA

Introduction: Brain tissue-derived extracellular vesicles (bdEVs) act locally in the central nervous system (CNS) and may indicate molecular mechanisms in HIV CNS pathology. Using brain homogenate (BH) and bdEVs from a simian immunodeficiency virus (SIV) model of HIV disease, we identified RNA networks in SIV infection and neuroinflammation.

Methods: Postmortem occipital cortex samples were obtained from uninfected controls and SIV-infected subjects (acute and chronic phases with or without CNS pathology (SIV encephalitis). bdEVs were separated and characterized per international consensus guidelines. RNAs from bdEVs and BH were sequenced and qPCR-amplified to detect levels of small RNAs (sRNAs, including microRNAs (miRNAs)) and longer RNAs including messenger RNAs (mRNAs) and circular RNAs (circRNAs).

*Corresponding author: Kenneth W. Witwer, kwitwer1@jhmi.edu; 733 North Broadway, Baltimore, MD 21205, USA

© The Author(s) 2023. Published by Oxford University Press on behalf of Infectious Diseases Society of America. All rights reserved. For permissions, please e-mail: journals.permissions@oup.com. This article is published and distributed under the terms of the Oxford University Press, Standard Journals Publication Model (<https://academic.oup.com/pages/standard-publication-reuse-rights>)

Results: Dysregulated RNAs in BH and bdEVs were identified in acute and chronic infection with pathology groups, including mRNAs, miRNAs, and circRNAs. Most dysregulated mRNAs in bdEVs reflected dysregulation in source BH. These mRNAs are disproportionately involved in inflammation and immune responses. Based on target prediction, several circRNAs that were differentially abundant in source tissue might be responsible for specific differences in sRNA levels in bdEVs during SIV infection.

Conclusions: RNA profiling of bdEVs and source tissues reveals potential regulatory networks in SIV infection and SIV-related CNS pathology.

Keywords: SIV, HIV, HAND, extracellular vesicles, bdEVs, miRNAs, mRNAs, circRNAs, exosomes, ectosomes, microvesicles

INTRODUCTION

Human immunodeficiency virus (HIV) infection causes chronic immune activation, inflammation, and end-organ diseases [1], including HIV-associated neurocognitive disorders (HAND) [2]. Studies of HIV neuropathology are facilitated by animal models. The SIV dual-inoculated pigtailed macaque (*Macaca nemestrina*) model, involving co-infection with a neurovirulent molecular clone SIV/17E-Fr and an immunosuppressive swarm SIV/DeltaB670, consistently recapitulates classic HIV CNS pathology [3,4].

Extracellular vesicles (EVs) may be involved in HIV-associated neuropathology as nano-sized membranous particles that share biogenesis pathways with HIV, affect virus entry, carry HIV components, and transfer molecules with pro-viral and anti-viral effects [5]. EVs can be used to assess the health of brain tissue and may betray disease if released into the periphery [6]. Recent advances allow rigorous separation and characterization of brain derived EVs (bdEVs) [7], whose molecular components may hint at mechanisms of CNS pathogenesis [7–9]. Previous studies of EV-associated messenger RNAs (mRNAs) [10] and microRNAs (miRNAs) [11,12] have suggested roles in HIV pathogenesis. In contrast, circular RNAs (circRNAs) [13]—highly stable, covalently closed single-stranded RNAs that may bind and modulate miRNAs as “sponges” [14] and compete with canonical mRNAs for splicing factors [15]—are relatively unexplored in HIV disease.

Here, we explored potential “competing endogenous RNA” (ceRNA) interactions in HIV infection. mRNAs, miRNAs, and circRNAs were measured by RNA sequencing (RNA-Seq) and quantitative PCR (qPCR) in brain homogenate (BH) and rigorously separated and characterized bdEVs in SIV CNS disease. We identified associations of specific RNA species. mRNA differences in BH and bdEVs largely correlated, while miRNA and circRNA findings suggest that several circRNAs may contribute to differential abundance of bdEV miRNAs.

METHODS

Tissues

Occipital cortex samples were from previous studies of male pigtailed macaques, approved by the Johns Hopkins Institutional Animal Care and Use Committee and conducted following the Weatherall Report, the Guide for the Care and Use of Laboratory Animals, and the USDA Animal Welfare Act. Occipital cortex samples (including both gray and white matter) were from subjects (Table 1) not infected (n=6) or dual-inoculated (n=16) with SIV swarm B670/clone SIV/17E-Fr [3,4] at acute (n=5, 7 days post-inoculation (dpi; peak of viral replication) and chronic infection (n=11, 84-101 dpi). Chronic cases were classified as [16,17] without or with CNS pathology (respectively: CP-, n=7; and CP+, SIV-encephalitis, n=4). For details of tissue perfusion, preparation, storage and pathological examination, see [3,4].

EV separation

bdEVs were separated [7–9] from 120–391 mg tissue (Table 1). ~50 mg was used for total RNA extraction (BH). The remainder was digested with 75 U/ml collagenase 3 (Worthington #CLS-3, S8P18814), 15 min, and spun at 300×g, 10 min and 2000×g, 15 min at 4°C. Supernatant was filtered (0.22 µm) and centrifuged at 10,000×g, 30 min at 4°C. Supernatant was separated by size exclusion chromatography (SEC) and concentrated and resuspended in 120 µl. For methodologic details, see [7].

Basic EV characterization

bdEV size profile and concentration were measured by nanoflow cytometry (NFCM; Flow NanoAnalyzer, NanoFCM, Inc.) as described [18].

Single particle interferometric reflectance imaging (SP-IRIS)

SP-IRIS was performed as described [18]. 10 µL bdEVs (from the 120 µl resuspension) were diluted in 35 µL incubation buffer (IB) and incubated overnight on ExoView tetraspanin chips (NanoView Biosciences). After 4 x 3 min washes in IB, chips were imaged (ExoView, NanoView) and data analyzed (NanoViewer 2.8.10, NanoView).

Transmission electron microscopy (TEM)

bdEVs (10 µL) were imaged as described [7] with a Philips CM120 instrument and an 8-megapixel AMT XR80 charge-coupled device.

Nucleic acid extraction

RNA was extracted from 100 µL bdEV resuspension with Trizol LS (Thermo Fisher 10296028). For tissue, Trizol (Thermo Fisher, 15596018) was used with Lysing Matrix D (MP Biomedicals, 116913100) and a benchtop homogenizer (FastPrep-24, MP Biomedicals). After homogenization,

RNA was isolated using miRNeasy solutions (Qiagen, 217004) with Zymo-Spin columns (Zymo Research, C1003–50). Genomic DNA was isolated using the AllPrep kit (Qiagen 80284) per manufacturer's recommendations.

Quantification of SIV RNA and total DNA (tdna)

Viral RNA was measured by quantitative PCR (qPCR, QuantiTect Virus kit, Qiagen 211011) or digital droplet PCR (ddPCR, One-Step RT ddPCR Advanced Kit for Probes, Bio-Rad 1864022). Copy numbers were calculated with a regression curve from control RNA transcripts. SIV total gag DNA (SIV gag tDNA) was measured by qPCR using Multiplex PCR Kit (Qiagen 206143).

Primers/probes: SIV21 forward 5'-GTCTGCGTCATCTGGTGCATTC-3'; SIV22 reverse 5'-CACTAGGTGTCTCTGCACTATCTGTTTTG-3'; SIV23, 5' FAM/3'-Black hole quencher-labeled probe 5'-CTTCCTCAGTGTGTTTCACTTTCTCTCTG-3' (Integrated DNA Technologies).

Two replications were performed for each sample and multiplexed with macaque beta interferon mac-IFN- β 2319 F FGCC TCA AGG ACA GGA TGA ACT T, mac-IFN- β 2294 R GCG TCC TCC TTC TGG AAC TG, and mac-IFN- β Probe CAT CCC TGA GGA AAT TAA GCA GCC GC for the quantitation of mac-IFN- β . Reaction mixtures were analyzed using a CFX96 Real-Time PCR Detection System (Bio-Rad): 95°C/10 minutes, 45 cycles of 95°C/15 seconds, 55°C/15 seconds, and 60°C/30 seconds. The number of cells per reaction was calculated by quantitating IFN- β DNA (two copies per cell) and used to normalize SIV gag RNA and tDNA from the same reaction.

Small RNA sequencing

Small RNA (sRNA) libraries (D-Plex Small RNA-seq, Diagenode, C05030001) were made from bdEV RNA (8 of 40 μ l RNA) or 20 ng BH RNA, using D-Plex Single Indexes for Illumina (Set A). After quality control by Fragment Bioanalyzer (DNA 1000, Agilent, 5067-1505), 170-230 bp libraries were selected by BluePippin (Sage Science, HTG3010). Multiplexed libraries were equally pooled to 1 nM and sequenced by NovaSeq 6000/SP Reagent Kit v1.5 (Illumina, 20028401, 100 cycles).

Srna sequencing data analysis

PolyA-tails and Illumina adapter sequences were removed by cutadapt (v3.4) and PCR duplicates were removed by collapsing identical sequences with seqkit. UMIs and template-switch motifs were removed further by cutadapt v3.4. All sequences shorter than 15 nt were discarded. The resulting reads were aligned to hg38 reference transcriptomes in a sequential manner using bowtie (v1.2.2, maximum 1 mismatch). Specifically, all reads were first mapped to mitochondrial chromosome (mtRNA) and house-keeping small non-coding RNAs with low sequence complexity, including rRNA, tRNA, RN7S, snRNA, sno/scaRNA, vault RNA, and RNY. The

unmapped reads were aligned sequentially to mature miRNA, pre-miRNA, protein-coding mRNA transcripts (mRNA), and long non-coding RNA (lncRNA). The raw counts for each transcript were extracted using eXpress (1.5.1) package. Scaled data (DESeq2) were visualized with principal component analysis (PCA). Differentially expressed (DE) sequences were defined as identified by both DESeq2 [19] and edgeR [20] with FDR-adjusted $p < 0.05$. RefFinder [21] was used to find internal reference genes. mRNA interaction/function prediction and cellular component annotations were from STRING [22]; hierarchical clustering by Heatmapper [23]; and miRNA-mRNA interactions by TargetScan [24] and miRDB [25]. Pearson's correlation was used to evaluate correlations. Two-tailed $p < 0.05$ was considered statistically significant. Analysis was conducted in R 4.2.1 and GraphPad Prism.

Total transcriptome sequencing

1 μ g BH RNAs was incubated with 1 U/ μ g RNase R (Lucigen, RNR07250) at 37°C, 30 min and purified by RNA Clean&Concentrator-5 (Zymo, R1014). cDNA libraries (100 ng RNA, with/without RNase R) were made with "IDT for Illumina RNA UD" indices by Stranded Total RNA Prep Ligation w/Ribo-Zero Plus (Illumina, 20072063). Yield/size distribution were assessed by Fragment Bioanalyzer (DNA 1000, Agilent 5067-1505). Libraries were pooled/sequenced as above.

Whole transcriptome sequencing data analysis

Illumina adapter sequences along with the first nucleotide of every read were removed with cutadapt v3.4, and fragments shorter than 15 nt were discarded. The trimmed and size-selected reads were aligned (Bowtie2 v2.3.4, default settings) to a manually curated *M. mulatta* mRNA reference (Mmul_10 Ensembl release 103) containing a single (main) transcript per gene (designated with gene symbols). Unaligned reads were mapped to combined *M. mulatta* mRNA/ncRNA references. Raw read counts aligned to each reference transcript were extracted using eXpress (1.5.1) [26].

Custom circrna sequential alignment (ciriseqa)

Trimmed and size-selected reads were first aligned to the *M. mulatta* reference transcriptome (Mmul_10, Ensembl release 103) as well as genomic DNA (Mmul_10 assembly) with bowtie (v1.2.2, default settings). After filtering non-circularized RNA fragments, reads were aligned to CircAtlas v.2 reference transcripts (<http://circatlas.biols.ac.cn>) containing putative circRNA junctions within each transcript. Raw read counts per transcript were then extracted using eXpress (1.5.1) [26] (Supplementary Figure 2).

Circexplorer2

Raw files were genome-aligned to the UCSC genome (BCM Mmul_8.0.1/rheMac8) using STAR, chimSegmentMin=10, and chimeric junction files were used to count circRNAs (circExplorer2).

circRNAs identified by both our custom circRNA sequential alignment (CiRISeqA) and circExplorer2 were included in the analysis.

Circrna data analysis

DE circRNAs were identified by edgeR (FDR<0.05=significant). miRanda [27] was used to predict circRNA-miRNA interactions (912 macaque miRNAs, miRBase).

Mirna qpcr

qPCRs (Thermo Fisher) were performed [12] for miRs-19a-3p (Assay 000395), 29a-3p (002112), 146a-5p (000468), 449a-5p (001030), and let-7a-5p (000377). Data were adjusted to the geomean Cq of internal references (as identified by RefFinder) miRs-124-3p (003188_mat), 125b-5p (000449), and 23b-3p (245306_mat).

Circrna qpcr

cDNA from 1 µg BH RNA or 5 µl bdEV RNA (iScript™ Reverse Transcription Supermix, Bio-Rad, 1708840) was amplified with iTaq Universal SYBRGreen Supermix (Bio-Rad 1725120). Divergent primers were designed (primer3, default parameters [28]) for circRNA junctions. Housekeeping reference was GAPDH for BH (forward 5'-CCATGGGGAAGGTGAAGGTC-3', reverse 5'-TGAAGGGGTCATTGATGGCA-3'), geomean Cq of the miRNAs listed above for bdEVs.

Statistical analysis, data availability, and EV-TRACK

Statistical significance was determined by Brown-Forsythe or Welch ANOVA tests. Sequencing data were deposited with GEO (transcriptome: GSE236937, sRNA: GSE236656). EV experimental details are found in EV-TRACK (EV230365) [29].

RESULTS

Occipital cortex bdEVs of uninfected and SIV-infected subjects (Figure 1; Table 1) were separated and characterized. sRNA-Seq was done for bdEVs and BH, while transcriptome sequencing was done for BH.

Particle counts, sizes, and morphology and brain SIV levels

bdEV preparation particle counts and size distributions suggested recovery of fewer particles from acute-phase samples versus uninfected and chronic infection without CNS pathology (SIV-encephalitis) (CP-; Figure 1B). Size distributions were similar (Figure 1C), while oval/round particles which consistent with EV morphology were revealed by TEM (Figure 1D). EV-

associated CD81, CD63, and CD9 were detected by SP-IRIS (Supplementary Figure 1). For infected subjects, SIV gag RNA and tDNA were detected in occipital cortex (Figure 1E), with more RNAs and tDNAs in CP+ vs CP-/Acute.

Bdev srnas in SIV infection and CP+

Ligation-independent sRNA-Seq of bdEVs yielded 38.7 million (M) (\pm 5.4M) reads/sample. 85.04% (\pm 1.81%) of processed bdEV reads mapped to the human genome. PCA (Figure 2A) indicated a clear separation of the acute group. For CP+ (n=4), three bdEV samples were separated from the other groups, while one was close to CP-. DE analysis of SIV versus uninfected and CP+ versus CP- (Figure 2B) found most differences between acute and uninfected (71 more, 6 less abundant), followed by CP+/uninfected (46 more, 2 less) and CP+/CP- (2 more abundant). No DE sRNAs were identified in CP-/uninfected. 38 DE sRNAs were consistently dysregulated in acute and CP+ versus uninfected; 2 were also dysregulated in CP+/CP- (Figure 2C). All 38 sRNAs were mapped to messenger RNAs (mRNAs), of which 30 had a high interaction confidence score (STRING, 0.7 on a scale of 0-1, Figure 2D). Gene ontology (GO) enrichment indicated involvement in immune regulation pathways (Figure 2E). Ten DE sRNAs (CP+ versus uninfected exclusively, Figure 2C, upper right) were visualized by unsupervised clustering (Figure 2F). Subjects in CP+ and uninfected groups clustered together (Figure 2F). Although no significant GO enrichment was found for these sRNAs, many have involvement in immune regulation based on DAVID [30], including protein tyrosine phosphatase (PTPRC), complement C7 (C7), IFI6 interferon alpha-inducible protein 6 (IFI6), CD74, and HLA-DRA.

Bdev mirna dysregulation in SIV and CP+

Because of relatively small sample size and our previous findings of miRNA dysregulation in biofluids during retroviral infection [12,31], we further ranked DE bdEV miRNAs based on unadjusted p-value. As for other sRNAs, there were more miRNA differences in acute versus uninfected (n=24) than for CP+/uninfected (n=14) or CP+/CP- (n=9) (Figure 3A and B). Only 3 miRNAs were dysregulated in both acute and CP+ versus uninfected, while 3 miRNAs were dysregulated in both CP+/uninfected and CP+/chronic (Figure 3B). Unsupervised clustering of 20 CP+-associated miRNAs suggested two miRNA clusters differed in CP+ and uninfected (Figure 3C). miRNA profiles of CP- are intermediate, with greater variance. qPCR confirmed that miR-19a-3p, let-7a-5p, and miR-29a-3p were less abundant during SIV infection (acute), and that miRs-146a-5p and -449a-5p were dysregulated in CP+ (Figure 3D).

BH circrna dysregulation in SIV infection and CP+

BHRNAs were sequenced with and without RNase R treatment to identify mRNAs and circRNAs. PCA of both mRNA and circRNA profiles (Figure 4A) showed separation of acute BH from other groups, and uninfected from the three infection groups, indicating an influence of SIV infection (Figure 4A). Mirroring bdEV findings, most DE mRNAs in BH were found in acute vs uninfected (n=245), followed by CP+/uninfected (n=78, Figure 4B). No DE mRNAs were identified in

CP+/CP- or CP-/uninfected. 69 mRNAs were consistently dysregulated in acute and CP+ versus uninfected (Figure 4B). The most DE circRNAs in BH were also found in the comparison of acute and uninfected (n=19), followed by CP+ versus uninfected (n=10), CP- versus uninfected (n=10), and CP+ versus CP- (n=4) (Figure 4B). However, only a few circRNAs were identified in more than one comparison (Figure 4B). Furthermore, linear RNAs corresponding to most DE circRNAs did not change significantly in SIV infection or CP+ (Figure 4C, grey). An exception was linear transcript IFI6, positively correlated with circ-IFI6_0001 (Figure 4C, red). qPCR confirmed dysregulation of circ-IFI6_0001, circ-EXOC2_0008, circ-PRKCE_0004, circ-PPP2R5A_0001, circ-RNF41_0003, and circ-ENC1_0001 in SIV-infected BH (Figure 4D).

Bdev versus BH rnas: SIV infection

sRNAs significantly different (FDR < 0.05) in both bdEVs and BH, acute versus uninfected (n=43, Figure 5A), and CP+ versus uninfected (n= 22, Figure 5B), were analyzed. A significant positive correlation of bdEVs and BH was observed for both acute vs uninfected (R=0.836, p<0.001) and CP+ vs uninfected (R=0.647, p=0.001) (Figures 5A and 5B). When comparing sRNA profiles between CP+ and CP-, two differentially abundant sRNAs, HLA-C and MX1, were identified only in bdEVs, not in BH. However, the pattern was consistent between bdEVs and BH, with a higher abundance in acute and CP+, and lower in uninfected and CP- (Supplementary Figure 3). Among six dysregulated BH circRNAs (Figure 4D), only circ-IFI6_0001 was found to be more abundant in CP+ for both bdEVs and BH by qPCR (Figure 5C). Its linear transcript, IFI6, was more abundant in acute and CP+ compared with uninfected (sequencing data), and for both bdEVs and BH (Figure 5C).

To identify possible ceRNA networks, qPCR-verified bdEV miRNAs (Figure 3D) and BH circRNAs (Figure 4D) were used for target prediction. miRanda predicted that three BH circRNAs (Figure 5D, blue) potentially bind with four bdEV miRNAs (Figure 5D, orange). The mRNA targets of these four miRNAs were predicted by TargetScan and miRDB (Supplementary Figure 4). These predicted mRNA targets were then compared with the mRNAs associated with infection, as determined by bdEVs sequencing data, resulting in the identification of four common mRNA targets (Figure 5D).

DISCUSSION

Roles of ceRNA networks in retrovirus-infected brain are largely undetermined. Here, we examined RNA profiles of bdEVs and BH in a model of HIV disease. Overall, sRNA and transcriptome differences were most pronounced in acute infection. However, important differences were also observed with chronic CNS pathology. Dysregulated mRNAs in bdEVs are involved in inflammation regulation and immune responses. Furthermore, ceRNA network analysis suggested that several brain circRNAs may affect bdEV miRNAs and mRNAs, warranting further investigation.

Whereas previous studies [31,32] report more abundant plasma EVs during SIV infection, particle concentrations were lower in acute bdEV preparations. Virions themselves are unlikely to explain overall EV abundance in plasma or brain: despite co-isolation with EVs [33], virions are insufficiently abundant even in acute infection to contribute to overall particle increases in plasma. Instead, cellular origins and uptake patterns in peripheral blood [6,34] and brain [8,35] may be responsible for the seemingly discrepant findings.

Previous studies of cell models revealed gene expression changes in HIV infection and HAND [36]. Here, acute infection and chronic pathology (CP+) samples, but not CP- samples, shared many mRNA differences, compared with uninfected. Eight signature bdEV mRNAs were dysregulated in CP+, encoding key immune system proteins, such as CD74 and HLA-DRA, involved in antigen processing and presentation [37], and interferon γ -inducible protein 16 (IFI16) [38], which modulates HIV transcription and latency reactivation [39] and senses retroviral DNA [38]. They are differentially abundant in both BH and bdEVs (Figure 5A-B), suggesting that CNS cells may use bdEVs to transfer antiviral elements.

miRNAs are also reportedly altered in HIV infection [40]. Here, several differences were verified by qPCR. Consistent with a previous report that let-7 miRNAs were less abundant in CD4+ T cells from HIV-1-infected progressors versus uninfected and long-term non-progressors, less let-7a-5p was found in acute phase bdEVs [41]. Since let-7 regulates PBMC immune responses via IL-10 [41] or other cytokines/chemokines [42], it could function similarly in CNS infection. miR-29a, previously found to be reduced in blood EVs during acute infection [31], may directly target HIV RNA to inhibit translation and replication [11], even during HIV latency [43]. Also correlated with SIV-associated CP were neuroinflammation-related miR-146a-5p [44] and brain development-related miR-449a-5p [45]. let-7a, miR-29a, and miR-449a were key components of a putative ceRNA network between BH and bdEVs (Figure 5D), indicating that levels in bdEVs, as well as those of target mRNAs, may be regulated by tissue circRNA expression.

Specific circRNAs that were DE not only in all infection groups compared with controls include qPCR-verified circ-PRKCE_0004, circ-PPP2R5A_0001, and circ-RNF41_0003, indicating persistent RNA dysregulation even in asymptomatic chronic infection. circ-IFI6_0001 and circ-EXOC2_0008 displayed dynamic changes during SIV infection/disease. circ-IFI6_0001 was more abundant in acute and CP+ groups but had similar levels in uninfected and CP- groups, while circ-EXOC2_0008 showed the reverse pattern. These differences indicate regulatory roles and biomarker potential in retroviral CNS infection. Among qPCR-verified circRNAs, circ-PRKCE_0004 and circ-ENC1_0001 may influence several bdEV miRNAs. Linear forms of some circRNAs have known function. IFI6 is an antiviral interferon-induced protein [46]. Exocyst Complex Component 2 (EXOC2) is involved in vesicle-mediated transport [47]. Both circular and linear IFI6 are consistently DE in BH and bdEVs, emphasizing that bdEVs may transfer viral infection regulators. Although several viruses reportedly to affect circRNAs [48], we know of only one publication on circRNA in HIV [13]. Our findings thus provide additional evidence of circRNA dysregulation in retroviral infection. Further studies are now needed into regulatory

mechanisms of these circRNAs in retroviral CNS infection and to assess biomarker and therapeutic potential.

In conclusion, we have identified mRNAs, miRNAs, and circRNAs linked to SIV infection and neuropathology, providing evidence of ceRNA network dysfunction in retroviral CNS disease. Our findings have several limitations: sample size was relatively small; the model may not recapitulate all aspects of HIV disease; not all targets were verified by qPCR; and different brain regions may be differently affected by viral infiltration and disease. Our results should thus be further explored and verified using larger cohorts, different brain regions, and in HIV infection.

Conflicts of interest: The authors report no conflicts of interest.

Acknowledgments: The authors thank members of the Witwer Laboratory for discussions and support. We are particularly grateful to members of the Retrovirus Laboratory for access to samples from the animal models and helpful suggestions. Electron microscopy images were acquired in the Johns Hopkins University School of Medicine Institute for Basic Biomedical Sciences Microscope Facility. RNA sequencing was performed in the Johns Hopkins University School of Medicine Single Cell & Transcriptomics Core.

Funding statement: This work was supported in part by the US National Institutes of Health, National Institute on Drug Abuse (NIDA, DA040385, and DA047807 to KWW), by two pilot grants awarded to YH through the Johns Hopkins NIMH Center (supported by MH075673) and the Johns Hopkins University Center for AIDS Research (supported by AI094189), and by NSF 2244127 to MB. The Witwer lab is also supported in part by NCI/Common Fund CA241694, NIAID AI144997, NIMH MH118164, and the Richman Family Precision Medicine Center of Excellence in Alzheimer's Disease. Samples used in this study were derived in part from research supported by U42OD013117 (Johns Hopkins, NIH supported pigtailed macaque breeding colony), NINDS NS089482 (to Joseph L. Mankowski), and NIMH MH070306 (to Janice E. Clements).

Meeting presentation: This work was presented at the International Society for Extracellular Vesicles (ISEV) 2023 Annual Meeting.

Corresponding author's contact information: Kenneth W. Witwer: kwitwer1@jhmi.edu, 733 North Broadway, Baltimore, MD 21205, USA

Author contributions: K.W.W., Y.H., and L.Z. conceived the idea. Y.H. performed most experiments and drafted and revised the manuscript text and figures; K.W.W. directed the project, obtained funding, supervised the experiments, and revised the manuscript; A.A., A.T., and M.B. performed small RNA and total RNA sequencing data analysis; S.Q. and C.M.A processed macaque brain samples and performed Gag RNA and total DNA qPCR; A.T. and X.Z. optimized figures. All authors read and approved the final manuscript.

References

1. Siliciano RF, Greene WC. HIV latency. *Cold Spring Harb Perspect Med*. 2011;1(1):a007096.
2. Smail RC, Brew BJ. HIV-associated neurocognitive disorder. *Handb Clin Neurol*. 2018;152:75-97.
3. Beck SE, Queen SE, Metcalf Pate KA, et al. An SIV/macaque model targeted to study HIV-associated neurocognitive disorders. *J Neurovirol*. 2018;24(2):204-212.
4. MC Z, K S, JL M, et al. High viral load in the cerebrospinal fluid and brain correlates with severity of simian immunodeficiency virus encephalitis. *J Virol*. 1999;73(12):10480-10488.
5. Madison MN, Okeoma CM. Exosomes: Implications in HIV-1 pathogenesis. *Viruses*. 2015;7(7):4093-4118.
6. Li Y, He X, Li Q, et al. EV-origin: Enumerating the tissue-cellular origin of circulating extracellular vesicles using exLR profile. *Comput Struct Biotechnol J*. 2020;18:2851.
7. Huang Y, Cheng L, Turchinovich A, et al. Influence of species and processing parameters on recovery and content of brain tissue-derived extracellular vesicles. *J Extracell Vesicles*. 2020;9(1):1785746.
8. Huang Y, Driedonks TAP, Cheng L, et al. Brain Tissue-Derived Extracellular Vesicles in Alzheimer's Disease Display Altered Key Protein Levels Including Cell Type-Specific Markers. *J Alzheimers Dis*. 2022;90:1057-1072.
9. Huang Y, Driedonks TAP, Cheng L, et al. Relationships of APOE Genotypes With Small RNA and Protein Cargo of Brain Tissue Extracellular Vesicles From Patients With Late-Stage AD. *Neurol Genet*. 2022;8(6):e200026.
10. Biswas S, Haleyrigirisetty M, Ragupathy V, et al. Differentially expressed host long intergenic noncoding RNA and mRNA in HIV-1 and HIV-2 infection. *Sci Rep*. 2018;8(1):2546.
11. Sun G, Li H, Wu X, et al. Interplay between HIV-1 infection and host microRNAs. *Nucleic Acids Res*. 2012;40:2181-2196.
12. Witwer KW, Sarbanes SL, Liu J, Clements JE. A plasma microRNA signature of acute lentiviral infection: Biomarkers of central nervous system disease. *AIDS*. 2011;25:2057-2067.
13. Zhang Y, Zhang H, An M, et al. Crosstalk in competing endogenous RNA networks reveals new circular RNAs involved in the pathogenesis of early HIV infection. *J Transl Med*. 2018;16:332.
14. Liu CX, Chen LL. Circular RNAs: Characterization, cellular roles, and applications. *Cell*. 2022;185:2016-2034.
15. Zhang Y, Zhao Y, Liu Y, et al. Exploring the regulatory roles of circular RNAs in Alzheimer's disease. *Transl Neurodegener*. 2020;9(1):35.
16. Mankowski JL, Clements JE, Zink MC. Searching for clues: tracking the pathogenesis of human immunodeficiency virus central nervous system disease by use of an accelerated, consistent simian immunodeficiency virus macaque model. *J Infect Dis*. 2002;186 Suppl 2:S199-S208.
17. Mangus LM, Dorsey JL, Laast VA, et al. Neuroinflammation and virus replication in the spinal cord of simian immunodeficiency virus-infected macaques. *J Neuropathol Exp Neurol*. 2015;74:38-47.
18. Arab T, Mallick ER, Huang Y, et al. Characterization of extracellular vesicles and synthetic nanoparticles with four orthogonal single-particle analysis platforms. *J Extracell Vesicles*. 2021;10(6):e12079.
19. Love MI, Huber W, Anders S. Moderated estimation of fold change and dispersion for RNA-seq data with DESeq2. *Genome Biol*. 2014;15:550.
20. Smyth GK, Ritchie ME, Law CW, et al. RNA-seq analysis is easy as 1-2-3 with limma, Glimma and edgeR. *F1000Res*. 2018;5:ISCB Comm J-1408.

21. Xie F, Wang J, Zhang B. RefFinder: a web-based tool for comprehensively analyzing and identifying reference genes. *Funct Integr Genomics*. 2023;23(2):125.
22. Szklarczyk D, Gable AL, Lyon D, et al. STRING v11: Protein-protein association networks with increased coverage, supporting functional discovery in genome-wide experimental datasets. *Nucleic Acids Res*. 2019;47:D607–D613.
23. Babicki S, Arndt D, Marcu A, et al. Heatmapper: web-enabled heat mapping for all. *Nucleic Acids Res*. 2016;44:W147–W153.
24. McGeary SE, Lin KS, Shi CY, et al. The biochemical basis of microRNA targeting efficacy. *Science*. 2019; 366(6472):eaav1741.
25. Chen Y, Wang X. miRDB: an online database for prediction of functional microRNA targets. *Nucleic Acids Res*. 2020;48:D127–D131.
26. Roberts A, Pachter L. Streaming fragment assignment for real-time analysis of sequencing experiments. *Nat Methods*. 2013;10:71–73.
27. Betel D, Koppal A, Agius P, et al. Comprehensive modeling of microRNA targets predicts functional non-conserved and non-canonical sites. *Genome Biol*. 2010;11(8):R90.
28. Untergasser A, Cutcutache I, Koressaar T, et al. Primer3--new capabilities and interfaces. *Nucleic Acids Res*. 2012;40(15):e115.
29. Van Deun J, Mestdagh P, Agostinis P, et al. EV-TRACK: Transparent reporting and centralizing knowledge in extracellular vesicle research. *Nat Methods*. 2017;14(3):228-232.
30. Sherman BT, Hao M, Qiu J, et al. DAVID: a web server for functional enrichment analysis and functional annotation of gene lists (2021 update). *Nucleic Acids Res*. 2022;50:W216–W221.
31. Huang Y, Liao Z, Dang P, et al. Longitudinal characterization of circulating extracellular vesicles and small RNA during simian immunodeficiency virus infection and antiretroviral therapy. *AIDS*. 2023;37(5):733-744.
32. Hubert A, Subra C, Jenabian MA, et al. Elevated abundance, size, and MicroRNA content of plasma extracellular vesicles in viremic HIV-1+ patients: Correlations with known markers of disease progression. *J Acquir Immune Defic Syndr*. 2015;70(3):219-227.
33. Hoen EN, Cremer T, Gallo RC, et al. Extracellular vesicles and viruses: Are they close relatives? *Proc Natl Acad Sci U S A*. 2016;113(33):9155-916.
34. Auber M, Svenningsen P. An estimate of extracellular vesicle secretion rates of human blood cells. *J Ex Bio*. 1(6):e46.
35. Huang Y, Arab T, Russell AE, et al. Toward a human brain extracellular vesicle atlas: Characteristics of extracellular vesicles from different brain regions, including small RNA and protein profiles. *Interdiscip. Med*. 2023, 1, e20230016.
36. Chang ST, Sova P, Peng X, et al. Next-generation sequencing reveals HIV-1-mediated suppression of T cell activation and RNA processing and regulation of noncoding RNA expression in a CD4+ T cell line. *mBio*. 2011;2(5):e00134-11.
37. Karakikes I, Morrison IEG, O'Toole P, et al. Interaction of HLA-DR and CD74 at the cell surface of antigen-presenting cells by single particle image analysis. *FASEB J*. 2012; 26(12):4886–4896.
38. Altfeld M, Gale M. Innate immunity against HIV-1 infection. *Nat Immunol*. 2015;16(6):554-562.
39. Hotter D, Bosso M, Jønsson KL, et al. IFI16 Targets the Transcription Factor Sp1 to Suppress HIV-1 Transcription and Latency Reactivation. *Cell Host Microbe*. 2019; 25(6):858-872.
40. Swaminathan S, Murray DD, Kelleher AD. The role of microRNAs in HIV-1 pathogenesis and therapy. *AIDS*. 2012; 26(11):1325–1334.

41. Swaminathan S, Suzuki K, Seddiki N, et al. Differential Regulation of the Let-7 Family of MicroRNAs in CD4+ T Cells Alters IL-10 Expression. *J Immunol.* 2012;188(12):6238-6246.
42. Venkatachari NJ, Jain S, Walker L, et al. Transcriptome analyses identify key cellular factors associated with HIV-1-associated neuropathogenesis in infected men. *AIDS.* 2017; 31(5):623–633.
43. Patel P, Ansari MY, Bapat S, et al. The microRNA miR-29a is associated with human immunodeficiency virus latency. *Retrovirology.* 2014; 11:108.
44. Zhao W, Spiers JG, Vassileff N, et al. microRNA-146a modulates behavioural activity, neuroinflammation, and oxidative stress in adult mice. *Mol Cell Neurosci.* 2023; 124:103820.
45. Wu J, Bao J, Kim M, et al. Two miRNA clusters, miR-34b/c and miR-449, are essential for normal brain development, motile ciliogenesis, and spermatogenesis. *Proc Natl Acad Sci U S A.* 2014; 111(28):E2851-E2857.
46. Kubo Y, Yasui K, Izumida M, et al. IDO1, FAT10, IFI6, and GILT Are Involved in the Antiretroviral Activity of γ -Interferon and IDO1 Restricts Retrovirus Infection by Autophagy Enhancement. *Cells.* 2022; 11(14):2240.
47. Bergen NJ van, Ahmed SM, Collins F, et al. Mutations in the exocyst component EXOC2 cause severe defects in human brain development. *J Exp Med.* 2020;217(10):e20192040.
48. Xie H, Sun H, Mu R, et al. The role of circular RNAs in viral infection and related diseases. *Virus Res.* 2021;291:198205.

Table 1. Subject characteristics.

Animal number	Animal ID	Group	Inoculation	SIVE*	Necropsy (dPI)	Age at Necropsy	Brain Weight (mg)
1	332	Uninfected	9/6/2011 (sham)	None	85	5	141
2	333	Uninfected	9/6/2011 (sham)	None	84	5.1	218
3	334	Uninfected	9/6/2011 (sham)	None	84	5.5	194
4	373	Uninfected	9/16/2014 (sham)	None	84	3.5	295

5	374	Uninfected	9/16/2014 (sham)	None	85	3.5	318
6	375	Uninfected	9/16/2014 (sham)	None	86	3.4	391
7	275	Acute	12/2/2008	None	7	3	246
8	282	Acute	12/2/2008	None	7	3.3	133
9	278	Acute	12/8/2008	None	7	3.3	253
10	284	Acute	12/9/2008	None	7	3.5	217
11	296	Acute	12/9/2008	None	7	2.3	168
12	262	CP-	11/19/2007	None	95	3.3	239
13	260	CP-	11/19/2007	None	101	3.4	298
14	294	CP-	7/25/2008	None	87	2.2	245
15	292	CP-	7/25/2008	None	84	3.2	120
16	299	CP-	4/6/2009	None	98	3	144
17	272	CP-	4/29/2010	None	84	4.7	298
18	351	CP-	11/20/2012	None	87	5.4	211
19	143	CP+	5/20/2005	+	208	3.9	204
20	295	CP+	7/25/2008	+	88	3	163

21	298	CP+	4/6/2009	+	93	3.1	211
22	350	CP+	11/20/2012	+	86	5.5	224

*SIVE: SIV encephalitis

FIGURE LEGENDS

Figure 1. Enrichment and characterization of bdEVs from uninfected and SIV-infected brain. A) Workflow for bdEV enrichment and RNA sequencing. bdEVs and brain homogenate (BH) were subjected to sRNA-Seq, while BH was subjected to transcriptome RNA-Seq. Created with BioRender.com. B) Particle concentrations of bdEVs from uninfected, acute, CP-, and CP+ samples (NFCM) normalized by tissue mass (per 100 mg). Data are presented as mean \pm SD. * $p \leq 0.05$, ** $p \leq 0.01$ by two-tailed Welch's t-test. C) bdEV size distributions (NFCM) presented in 5-nm size bins versus total detected particles/sample (percentage). D) bdEVs visualized by negative staining transmission electron microscopy (TEM) (scale bar=500 nm); TEM is representative of ten images taken of each fraction from three independent tissue samples. E) SIV viral Gag RNA and total DNA (tDNA) as copy number/ 10^6 cells in occipital cortex. Data are presented as mean \pm SD. LOD (limit of detection). * $p \leq 0.05$ by two-tailed Welch's t-test.

Figure 1

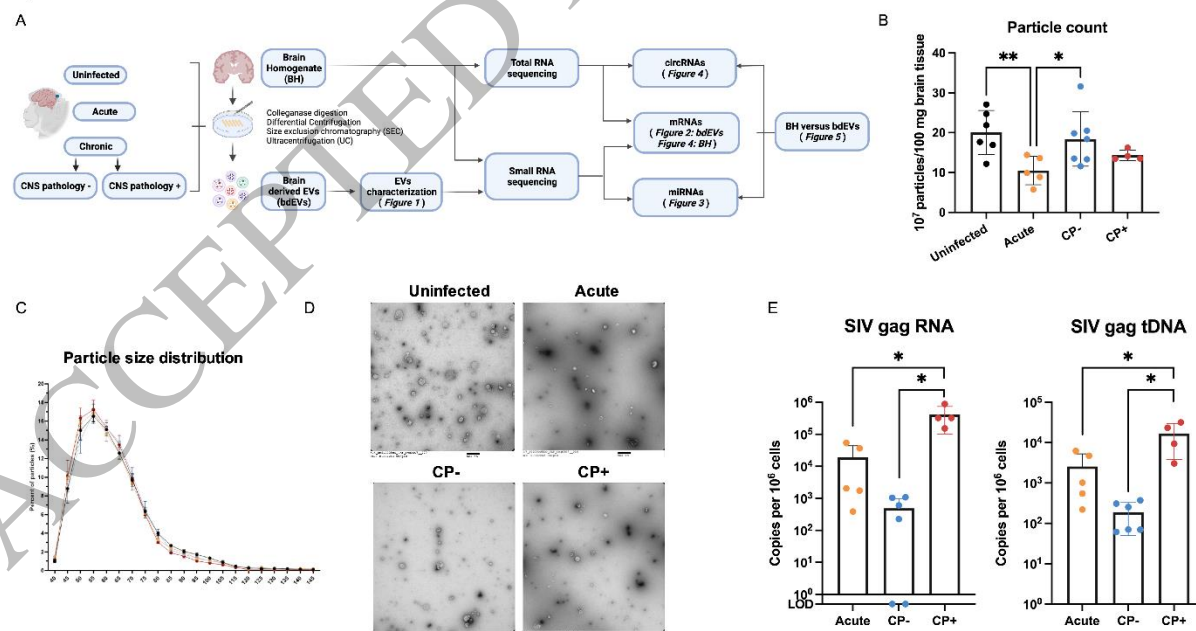


Figure 2. bdEV sRNAs with differential expression in SIV infection. A) Principal component analysis (PCA) using bdEV sRNA profiles of uninfected, acute, CP-, and CP+ groups. Animal #299 in the CP- group was defined as an outlier and is not shown. B) Numbers of DE sRNAs in

group comparisons, based on adjusted $p < 0.05$ by both DESeq2 and edgeR. C) Venn diagrams of DE sRNAs in acute and CP+ versus uninfected and CP+ versus CP-. D) STRING protein interaction network analysis: 30 of 38 mRNAs dysregulated in both acute and CP+ groups had a high interaction confidence score (0.7 on a scale of 0-1). E) Top 10 biological processes (GO enrichment) ranked by FDR-corrected p-value for 38 mRNAs dysregulated in both acute and CP+ groups. F) Unsupervised hierarchical clustering of 10 DE bdEV sRNAs (CP+ versus uninfected).

Figure 2

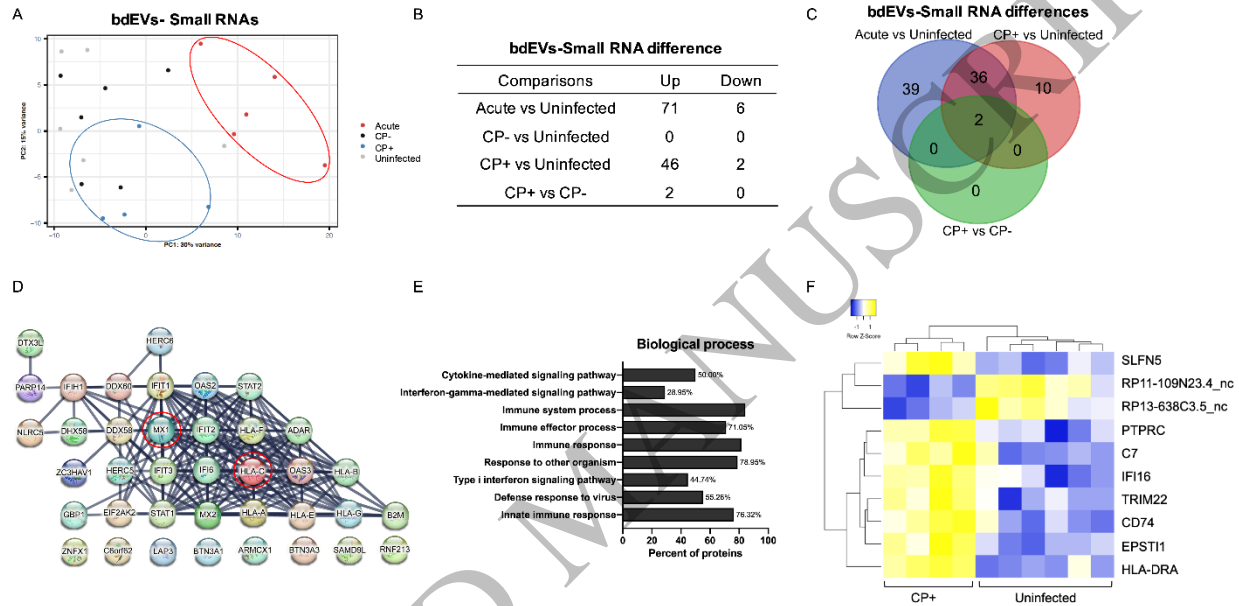


Figure 3. DE bdEV miRNAs in SIV infection. A) Volcano plots of bdEV miRNA log₂FC and p-value for acute/uninfected (left), CP+/uninfected (middle), and CP+/CP- (right). Dashed lines: thresholds for 2-fold change and $p < 0.05$. Significance indicated as gray=not significant, red=non-adjusted $p < 0.05$. B) Venn diagrams of DE miRNAs (non-adjusted $p < 0.05$) in acute and CP+ versus uninfected and CP+ versus CP-. C) Unsupervised hierarchical clustering of 20 DE bdEV miRNAs of CP+ versus CP- and uninfected. D) qPCR validation for bdEV miR-19a-3p, let-7a-5p, miR-29a-3p, miR-146a-5p, and miR-449a-5p. DeltaCq values were normalized to the geometric mean Cq value of internal references: miR-124-3p, miR-125b-5p, and miR-23b-3p. Data are presented as mean \pm SD. * $p \leq 0.05$, ** $p \leq 0.01$ by two-tailed Welch's t-test.

Figure 3

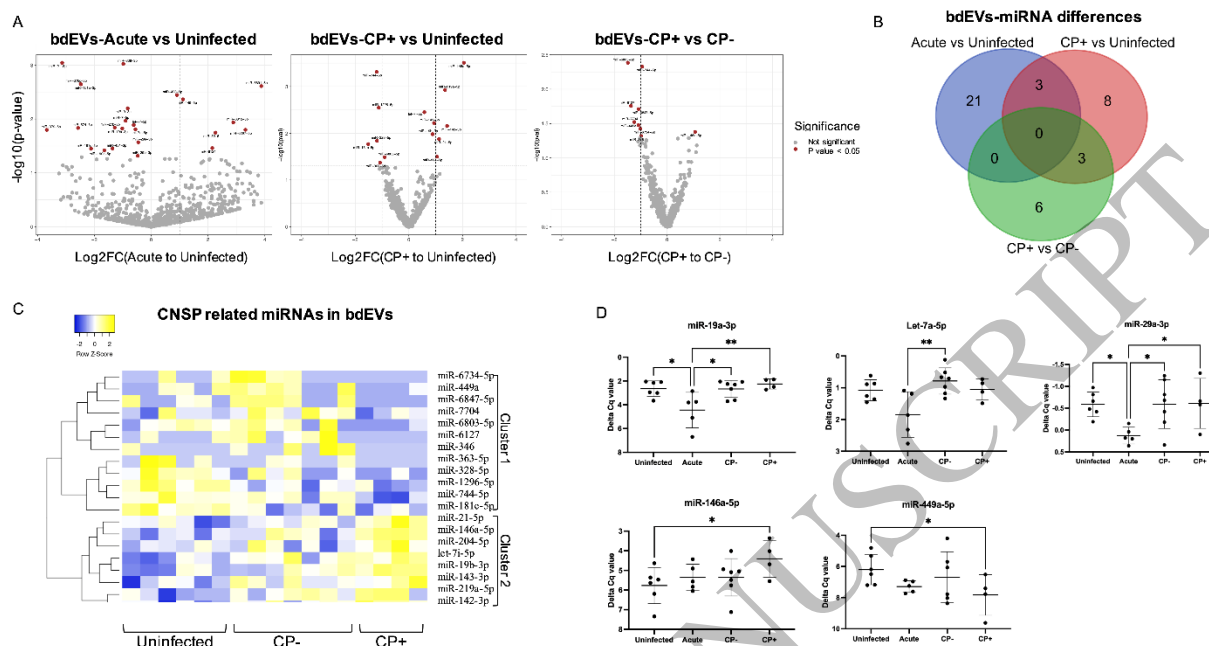


Figure 4. circRNA dysregulation in SIV-infected brain tissues. A) Multidimensional scaling analysis based on quantitative mRNA (left) and circRNA (right) BH profiles. B) Venn diagrams of differentially abundant mRNAs (left) and circRNAs (right) (adjusted $p < 0.05$) in acute, CP+, and CP- groups versus uninfected and CP+ versus CP-. C) Log₂FC of circRNAs and corresponding linear mRNAs. Red dots: both circRNA and corresponding linear RNA are DE between groups, with adjusted $p < 0.05$. D) qPCR validation of BH circ-IFI6_0001, circ-EXOC2_0008, circ-PRKCE_0004, circ-PPP2R5A_0001, circ-RNF41_0003, and circ-ENC1_0001. Delta Cq values were normalized to the Cq value of GAPDH. Data are presented as mean \pm SD. * $p \leq 0.05$, ** $p \leq 0.01$ by two-tailed Welch's t-test.

Figure 4

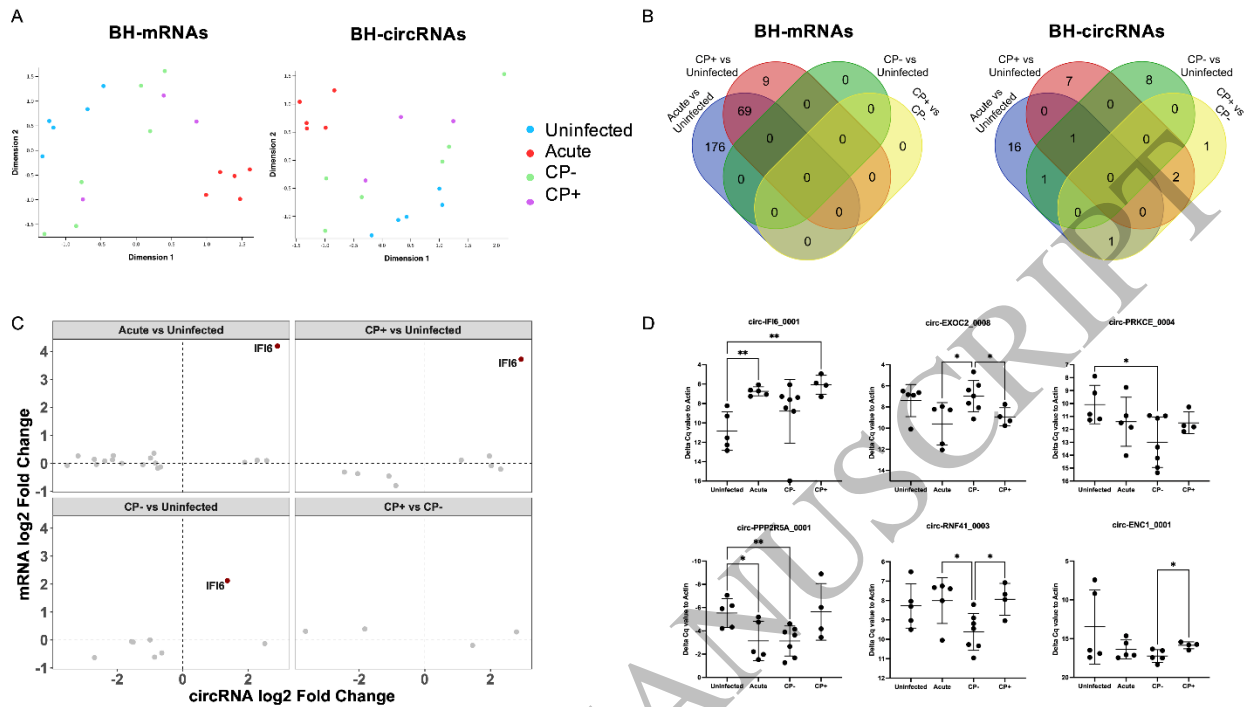


Figure 5. SIV-related mRNA and circRNA changes in bDEVs and BH. A) Correlations of sRNA log₂FC in bDEVs and BH: acute versus uninfected. The linear regression line is shown in black. Pearson's correlation coefficient (R) and significance (p) are shown for all DE siRNAs, acute versus uninfected. B) Correlations of sRNA log₂FC in bDEVs and BH, CP+ versus uninfected. The linear regression line is shown in black. Pearson's correlation coefficient (R) and significance (p) are shown for all DE sRNAs, CP+ versus uninfected. C) Levels of circ-IFI6_0001(left) and IFI6 (right) in bDEVs and BH. *adjusted p<0.05 per edgeR. D) Putative ceRNA network. The blue rectangle nodes represent circRNAs, the orange oval nodes represent miRNAs, and the green hexagon nodes denote mRNAs. Edges are interactions between RNAs.

Figure 5

